Xiang *et al. Chin. J. Mech. Eng.* (2019) 32:41
https://doi.org/10.1186/s10033-019-0359-1

Chinese Journal of Mechanical Engineering

ORIGINAL ARTICLE Open Access

A Contact Force Model Considering Meshing and Collision States for Dynamic Analysis in Helical Gear System

Dong Xiang, Yinhua Shen* and Yaozhong Wei

Abstract

The current research on gear system dynamics mainly utilizes linear spring damping model to calculate the contact force between gears. However, this linear model cannot correctly describe the energy transfer process of collision that often occurs in gear system. Focus on the contact-impact events, this paper proposes an improved gear contact force model for dynamic analysis in helical gear transmission system. In this model, a new factor associated with hysteresis damping is developed for contact-impact state, whereas the traditional linear damping factor is utilized for normal meshing state. For determining the selection strategy of these two damping factors, the fundamental contact mechanics of contact-impact event affected by supporting forces are analyzed. During this analysis, an effect factor is proposed for evaluating the influence of supporting forces on collision. Meanwhile, a new restitution of coefficient is deduced for calculating hysteresis damping factor, which suitable for both separation and non-separation states at the end of collision. In addition, the time-varying meshing stiffness (TVMS) is obtained based on the potential energy approach and the slice theory. Finally, a dynamic analysis of a helical gear system is carried out to better understand the contact force model proposed in this paper. The analysis results show that the contribution of supporting forces to the dynamic response of contact-impact event within gear pair is important. The supporting forces and dissipative energy are the main reasons for gear system to enter a steady contact state from repeated contact-impact state. This research proposes an improved contact force model which distinguishes meshing and collision states in gear system.

Keywords: Contact-impact event, Gear transmission, Contact force, Restitution coefficient, Flexible support

1 Introduction

The contact force model plays a key role in predicting the response of multibody mechanical system since it has a significant influence on the response of the system [1]. As a typical multibody system, the gear transmission system is widely used in engineering application, such as aircrafts, marine ships, automobiles, wind turbines, etc. The contact force between gears is mainly calculated by linear spring damping model [2–4] which consists of two mass elements, two spring elements, and a damping element. Khulief and Shabana [5] applied this model to dynamic analysis in multibody system, and Kahraman and Singh [6] earlier used it to analyze the dynamic characteristics of a single degree freedom gear system combined with error excitation. After that, scholars carried out further researches for gear transmission based on the linear model [7–11].

The damping term in the linear model, which utilized to describe the energy loss during meshing process, is obtained based on the oscillation decay period of the linear spring damping system. However, reference [12] presents that this damping term cannot correctly describe the energy transfer process for the contact-impact event which frequently occurs in gear system. Instead, a nonlinear impact damping model [12] is employed for collision analysis, which is proposed according to restitution coefficient to describe the dissipated energy during contact-impact event. Based on this coefficient of restitution, other improved models are also established, such as the Lee and Wang model [13], the Lankarani and Nikravesh

*Correspondence: syhua_2001@163.com
Department of Mechanical Engineering, Tsinghua University, Beijing 100084, China

model [14], the Gharib and Hurmuzlu model [15], the Flores et al. model [1], the Hu and Guo model [16], etc.

These nonlinear models mentioned before are mostly derived from two free impact-contact bodies. However, the gear pair is supported by bearings which are often described as spring elements in dynamics model. This indicates that the contact-impact event between gears is affected by supporting forces during simulation, thus, the governing motion equations of gear system contain the balance between contact-impact force and supporting forces. When the influence of supporting forces is large enough, these nonlinear models may exhibit obvious errors for the dynamic response of gear system [17, 18]. Particularly, the accumulation of these errors of repeated or sustained contact-impact event which frequently take place in gear system can cause the distortion simulation in gear dynamics. In addition, these nonlinear models cannot be used to correctly calculate the energy loss during normal meshing process since they are only suitable for one single collision.

The purpose of this paper is to propose an improved contact force model for dynamic analysis of helical gear transmission system. In this model, different contact force models are applied in conjunction with TVMS to calculate the meshing and contact-impact forces, respectively. In order to determine the strategy for choosing these force models, the effect of external forces on collision is investigated, and then the judgment of impact end states, namely separation and non-separation, is deduced. Meanwhile, an impact damping factor associated with Newton method is developed based on an improved restitution coefficient deduced by considering the two impact end states. Finally, the performance of this improved gear contact force model is analyzed with a simulation of a helical gear system.

2 Stiffness and Damping

In literatures, the gear contact force along the line of action is usually characterized by TVMS and meshing damping, as shown in Eq. (1):

$$F_n = \begin{cases} k_m(\delta - b) + D\dot{\delta}, & \delta > b, \\ 0, & -b \le \delta \le b, \\ k_m(\delta + b) - D\dot{\delta}, & \delta < -b, \end{cases} \tag{1}$$

where k_m and D indicate the TVMS and damping factor, respectively, δ denotes the relative displacement between contact point, $\dot{\delta}$ illustrates the relative velocity and $2b$ is the backlash between gears. For Eq. (1), the calculations of stiffness and damping are the two important tasks.

2.1 Time-Varying Meshing Stiffness

The gear TVMS is a key parameter of gear dynamic model, and many studies have been carried out to calculate this stiffness. The finite element method (FEM) has high enough accuracy to simulate the actual gear tooth profile and calculate automatically the contact position, thus, it is utilized popularly for the TVMS [19, 20]. However, the FEM is complicated and requires a lot of computing resources. Differently, the analytical method (AM) is a simple and efficient approach for calculating TVMS. In AM, the potential energy method represented by Yang and Li [21] is used. According to this method, the meshing stiffness of spur gear pair is composed of tooth stiffness, tooth radial compressive stiffness, tooth shear stiffness, Hertzian contact stiffness and gear foundation stiffness. For helical gear pair, the slice theory is applied popularly, in which the helical gear is regarded as a series of spur gear slices [22, 23]. Thus, the transverse meshing stiffness of the helical gear pair can be obtained by integration along tooth width direction. Additionally, the meshing stiffness of the helical gear pair also contains axial tooth stiffness and axial gear foundation stiffness, and hence this meshing stiffness can be given by

$$k_m = \frac{1}{\cos\beta_b/k_t + \sin\beta_b/k_a}, \tag{2}$$

where k_t and k_a illustrate the transverse meshing stiffness and axial meshing stiffness, respectively, and β_b indicates the base helix angle. According to the slice theory, the transverse meshing stiffness is obtained by integrating slice cylindrical spur gear pair along the mesh line, which can be expressed as

$$k_t = \sum_{i=1}^{n} \frac{1}{1/k_{h,i} + 1/k_{ta1,i} + 1/k_{tb1,i} + 1/k_{ts1,i} + 1/k_{tf1,i} + 1/k_{ta2,i} + 1/k_{tb2,i} + 1/k_{ts2,i} + 1/k_{tf2,i}} \tag{3}$$

with

$$k_n = \frac{\pi E \Delta l}{4\left(1-\nu^2\right)}, \tag{4}$$

$$\frac{1}{k_{ta}} = \int_{\pi/2}^{\alpha} \frac{\sin^2\varphi}{EA_{y1}} \frac{\mathrm{d}y_1}{\mathrm{d}\gamma}\mathrm{d}\gamma + \int_{\tau_c}^{\varphi} \frac{\sin^2\varphi}{GA_{y2}} \frac{\mathrm{d}y_2}{\mathrm{d}\tau}\mathrm{d}\tau, \tag{5}$$

$$\frac{1}{k_{tb}} = \int_{\pi/2}^{\alpha} \frac{\left[\cos\varphi\left(y_\varphi - y_1\right) - x_\varphi \sin\varphi\right]^2}{EI_{y1}} \frac{\mathrm{d}y_1}{\mathrm{d}\gamma}\mathrm{d}\gamma + \int_{\tau_c}^{\varphi} \frac{\left[\cos\varphi\left(y_\varphi - y_2\right) - x_\varphi \sin\varphi\right]^2}{EI_{y2}} \frac{\mathrm{d}y_2}{\mathrm{d}\tau}\mathrm{d}\tau, \tag{6}$$

$$\frac{1}{k_{ts}} = \int_{\pi/2}^{\alpha} \frac{1.2\cos^2\varphi}{GA_{y1}} \frac{\mathrm{d}y_1}{\mathrm{d}\gamma}\mathrm{d}\gamma + \int_{\tau_c}^{\varphi} \frac{1.2\cos^2\varphi}{GA_{y2}} \frac{\mathrm{d}y_2}{\mathrm{d}\tau}\mathrm{d}\tau, \tag{7}$$

$$k_{tf} = \frac{\cos^2\varphi}{E\Delta l}\left\{L^*\left(\frac{u_f}{s_f}\right)^2 + M^*\left(\frac{u_f}{s_f}\right) + P^*\left(1 + Q^*\tan^2\varphi\right)\right\}, \tag{8}$$

where k_h indicates the contact stiffness of the slice tooth pair, k_{ta}, k_{tb}, k_{ts} and k_{tf} are the slice tooth radial compressive stiffness, slice tooth bending stiffness, slice tooth shear stiffness and slice gear foundation stiffness, respectively. The symbols E, ν and Δl illustrate Young's modulus, Poisson's ratio and slice tooth width, respectively. α represents the transverse operation pressures angle, ϕ is the pressure angle of the contact point. Parameters x_ϕ, y_ϕ, y_1, y_2, $\mathrm{d}y_1/\mathrm{d}\gamma$ and $\mathrm{d}y_2/\mathrm{d}\tau$ are listed in Ref. [24], whereas u_f, S_f, L^*, M^*, P^* and Q^* are shown in Ref. [25]. A_{y1}, A_{y2}, I_{y1} and I_{y2} can be calculated as follows:

$$A_{y1} = 2x_1\Delta l, \quad A_{y2} = 2x_2\Delta l, \tag{9}$$

$$I_{y1} = \frac{2x_1^3\Delta l}{3}, \quad I_{y2} = \frac{2x_2^3\Delta l}{3}, \tag{10}$$

where x_1 and x_2 can also be found in Ref. [24].

For the axial meshing stiffness, Ref. [23] represents a detailed solution process and the results are given by

$$k_a = \frac{1}{1/k_{ab} + 1/k_{at} + 1/k_{af}} \tag{11}$$

with

$$\frac{1}{k_{ab}} = \int_{\pi/2}^{\alpha} \frac{\left(y_\varphi - y_1\right)^2}{EI_{x1}} \frac{\mathrm{d}y_1}{\mathrm{d}\gamma}\mathrm{d}\gamma + \int_{\tau_c}^{\varphi} \frac{\left(y_\varphi - y_1\right)^2}{EI_{x2}} \frac{\mathrm{d}y_2}{\mathrm{d}\tau}\mathrm{d}\tau, \tag{12}$$

$$\frac{1}{k_{at}} = \int_{\pi/2}^{\alpha} \frac{x_\varphi^2}{GI_{p1}} \frac{\mathrm{d}y_1}{\mathrm{d}\gamma}\mathrm{d}\gamma + \int_{\tau_c}^{\varphi} \frac{x_\varphi^2}{GI_{p2}} \frac{\mathrm{d}y_2}{\mathrm{d}\tau}\mathrm{d}\tau, \tag{13}$$

$$\frac{1}{k_{af}} = \int_{0}^{r_f} \frac{\left(y_\varphi - y\right)}{EI_{af}}\mathrm{d}\gamma, \tag{14}$$

where k_{ab} and k_{at} represent the axial tooth bending stiffness and axial tooth torsional stiffness, respectively, and k_{af} indicates the axial gear foundation stiffness. I_{x1}, I_{x2}, I_{p1} and I_{p2} can be obtained by

$$I_{x1} = \frac{1}{6}B^3x_1, \quad I_{x2} = \frac{1}{6}B^3x_2, \tag{15}$$

$$I_{p1} = \frac{1}{6}\left(4Bx_1^3 + B^3x_1\sec^2\varphi\right), \quad I_{p2} = \frac{1}{6}\left(4Bx_2^3 + B^3x_2\sec^2\varphi\right), \tag{16}$$

in which B denotes the tooth width.

2.2 Damping Factor for Meshing and Collision States

In addition to the TVMS, the meshing damping also has great effect on the dynamic behavior of the gear system. However, the meshing damping is difficult to evaluate due to it depends on complex mechanisms in the structure [26]. Generally, a simplified damping model is frequently used and it is given by

$$D = c_m = 2\zeta_m\sqrt{k_m\frac{J_pJ_g}{J_pR_g^2 + J_gR_p^2}}, \tag{17}$$

where J_p and J_g denote the rotary inertia of gears, R_p and R_g illustrate the gears base radius, and ζ_m is the damping coefficient. As the analysis shown in Ref. [27], the value of ζ_m is between 0.03 to 0.17.

This damping model shown in Eq. (17) is effective for calculating the energy loss at the gear meshing interface in normal meshing state, but it lacks sufficient accuracy for the dissipative energy during collision which frequently occurs in the gear system. An impact damping which is also called Hertzian damping is proposed for accurately computing this energy loss, and it also utilized for the contact-impact dynamics in the gear system [21, 28]. Eq. (18) shows a classical impact damping factor model which is propose by Hu and Guo, and other similar models can be found in Ref. [29].

$$D = \mu\delta^n = \frac{3(1-\varepsilon)}{2\varepsilon}\frac{k_m}{\dot{\delta}^{(-)}}\delta^n, \tag{18}$$

where μ is the hysteresis damping factor, ε denotes the coefficient of restitution, and $\dot{\delta}^{(-)}$ indicates the initial relative velocity between impact bodies. In addition, the value of the exponent n is taken as 1 in this paper.

However, these existing impact damping models are deduced based on Newton law coefficient of restitution which cannot be used for the collision affected by external forces, thus, it is important to analyze the influence of supporting forces on collision for improving impact

damping model. As mentioned earlier, these impact damping models only describe the energy loss of a single collision process, and it may exhibit obvious error for normal gear mesh process. To obtained accurate dynamics of gear system, it is necessary to utilize different damping models for different gear pair states, including meshing process and impact process. For this purpose, the essential problem is to analyze the end state of the collision, so as to determine the conversion of different damping models during simulation.

3 Impact Damping Model Considering Supporting Forces

An contact-impact model is employed for analysis, as shown in Figure 1 where the collision pair with masses m_i and m_j, and velocities $\dot{x}_i$ and $\dot{x}_j$, is also supported by springs (k_i, k_j) and dampers (c_i, c_j). According to Refs. [2, 3], the contact force during the contact-impact event is

$$F_n = k_m\delta + \mu\delta\dot{\delta}, \tag{19}$$

where δ is the local deformation, k_m denotes the contact stiffness, $\dot{\delta}$ represents the relative velocity, and μ is the hysteresis damping factor. It should be noted that the hysteresis damping factor μ must be determined.

3.1 Influence of Supporting Forces on Collision

The linear spring force model is used to estimate the influence of supporting forces on contact-impact event in this paper, therefore, the dynamic equivalent equation of the contact-impact system can be written in the following form

$$m_e\ddot{\delta} + k_m\delta = m_e a_e \tag{20}$$

where $m_e = m_i m_j/(m_i + m_j)$ represents the equivalent mass of these two bodies, a_e denotes the relative acceleration under the external forces and it is expressed as

$$a_e = \frac{F_i}{m_i} + \frac{F_j}{m_j}, \tag{21}$$

where F_i and F_j represent the supporting forces.

According to Refs. [17, 18], which have discussed the influence of external forces on collision, the maximum elastic strain energy, the deformation velocity and the energy loss can be expressed by Eqs. (22), (23), and (24), respectively, based on Eq. (20) and the separation end state of collision:

$$\frac{1}{2}k\delta_m^2 = \frac{1_i}{2(1-\xi)}m_e\left(\dot{\delta}^{(-)}\right)^2, \tag{22}$$

$$\dot{\delta} = \dot{\delta}^{(-)}\sqrt{1 - \left(\frac{\delta}{\delta_m}\right)^2 + \frac{\xi_c}{1-\xi_c}\left[\chi - \left(\frac{\delta}{\delta_m}\right)^2\right]}, \tag{23}$$

$$\Delta E = \left[\frac{1}{2(1-\xi_c)}m_e\left(\dot{\delta}^{(-)}\right)^2\right]\left(1-\varepsilon^2\right), \tag{24}$$

with

$$\xi_c = \frac{\int_0^{\delta_m} m_e a_e \mathrm{d}\delta}{\frac{1}{2}m_e\left(\dot{\delta}^{(-)}\right)^2 + \int_0^{\delta_m} m_e a_e \mathrm{d}\delta}, \tag{25}$$

where $\dot{\delta}^{(-)}$ denotes the initial relative velocity, χ is the ratio of the work done by equivalent supporting force $F_e = m_e a_e$ and its maximum value, δ_m and ΔE are the maximum compression and dissipated energy of collision, respectively.

Eqs. (22), (23), and (24) show that the maximum elastic strain energy, the deformation velocity, and the energy loss during collision increase as ξ_c increases when the initial relative velocity and equivalent mass are fixed. It should be highlight that the ratio ξ_c is associated with k_m, m_e, $\dot{\delta}^{(-)}$ and a_e. The value of ξ_c is less than 1 according to Eq. (25). When $\xi_c < 0$, the supporting forces weaken the compression of collision, whereas the case of $0 < \xi_c < 1$ illustrates the strengthening effect of supporting forces. In addition, $\xi_c = 0$ means the supporting forces are equal to zero, and $\xi_c = 1$ denotes there is no collision.

Similarly, the influence of supporting forces on restitution phase can be evaluated by the following formula

$$\xi_r = \frac{-\int_{\delta_m}^{0} m_e a_e \mathrm{d}\delta}{\frac{1}{2}m_e\left(\dot{\delta}^{(-)}\right)^2 - \int_{\delta_m}^{0} m_e a_e \mathrm{d}\delta}, \tag{26}$$

where $\dot{\delta}^{(+)}$ indicates the separation velocity right after collision. During restitution, the value of ξ_r is less than or equal to 1. The case $\xi_r = 1$ means the colliding bodies cannot separate at the end of collision. The supporting forces accelerate the restitution effect when $\xi_r < 0$, whereas the condition of $\xi_r > 0$ illustrates the prevention of the supporting forces on restitution. Therefore, the ratios ξ_c and ξ_r are defined as the effect factor of supporting force on collision.

As analyzed before, the non-separation state can occur when $\xi_r = 1$. This state is also the key to choose the

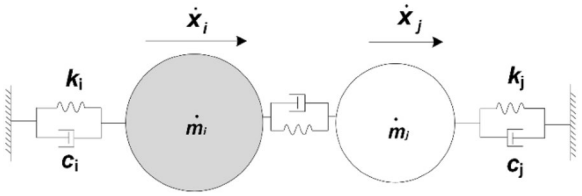

Figure 1 Contact-impact model under flexible support

different damping models for meshing state and impact state. Thus, the end state of collision and its judgement are illustrated.

Eq. (27) shows the energy balance in collision process, and its detail derivation can be found in Ref. [18]:

$$E_r^+ = E_r^- - (W_{er} - W_{ec}) - \Delta E, \tag{27}$$

where E_r^+ and E_r^- denotes the final relative kinetic energy and the initial relative kinetic energy, respectively, W_{ec} represents the work done by equivalent supporting force in compression phase, whereas W_{er} is in restitution phase. This expression denotes that if the initial relative kinetic energy E_r^- can satisfy all the energy consumption which consists of ΔE and $W_{er} - W_{ec}$ during contact-impact event, then $E_r^+ > 0$ and the collision pair enters separation state. The E_r^+ cannot be negative, hence, if $E_r^+ = 0$ and the colliding bodies still not separated, the collision pair enters non-separation state. Thus, the judgement of the contact-impact end state can be described as follows.

(1) During restitution phase, the collision pair enters separation state when $\delta = 0$ and $E_r^+ > 0$.
(2) During restitution phase, the collision pair enters non-separation state when $\delta > 0$ and $E_r^+ = 0$.

3.2 Coefficient of Restitution

In general, the coefficient of restitution plays a crucial role for deducing the impact damping model, and it had been indicated in Ref. [30] that the Newton model and Poisson model cannot obey the law of energy conservation when the energy loss during impact from sources other than friction. Instead, an energy model which is also called Stronge model is proposed, and it is defined as the square root of the ratio ε of the elastic strain energy released during restitution to the energy absorbed by deformation in compression. In terms of the work done by the contact force during the two phases, the restitution coefficient is

$$\varepsilon^2 = -\frac{W_r}{W_c}, \tag{28}$$

where W_c and W_r represent the work done by contact force during the compression and restitution phases, respectively.

In fact, this energy model is obtained based on the separation state, and it can exhibit obvious error for the non-separation state, as shown in Figure 2. This figure represents the development of the contact force during collision which is affected by an equivalent supporting force. It should be highlighted that the contact force is obtained by the liner spring model, this means there is no energy loss during collision and the coefficient of restitution should theoretically be equal to 1. However, the result obtained by Eq. (17) is about 0.89. Therefore, it is necessary to improve the model of the restitution coefficient, which can be applied to both the separation and the non-separation.

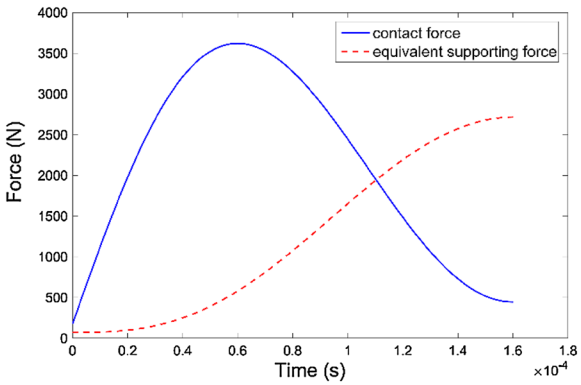

Figure 2 Influence of equivalent supporting force

According to Eq. (28), the energy loss for separation state can be given by

$$\Delta E = W_c + W_r = \left(1 - \varepsilon^2\right) W_c, \tag{29}$$

thus the restitution coefficient is derived as

$$\varepsilon^2 = \frac{W_c - \Delta E}{W_c}, \tag{30}$$

in which ΔE indicates the work done by damping force during impact-contact event.

Since the contact force model applied in Figure 2 does not contain damping force, the energy loss ΔE is equal to zero, and then the restitution coefficient calculated by Eq. (30) is equal to 1 which is the theoretical value. For the separation state, the result obtained by Eq. (30) is equal to Eq. (28). Hence, Eq. (30) is employed to deduce the impact damping model in this paper.

3.3 Impact Damping Model

As before analysis, the influence of supporting forces on collision cannot be ignored when these forces are large enough, and the existing impact damping models may exhibit obvious errors, as shown in Figure 3 which illustrates the plots of the pre-restitution coefficient represented in Table 1 and the post-restitution coefficient obtained by Eq. (30) with a continuous contact analysis. The straight line which represents the same value for post and pre- restitution coefficient is used as reference. This approach proposed by Lankarani and Nikravesh [14] is also adopted for analyzing the impact damping factor in Refs. [1, 16]. The results of Figure 3 indicate that

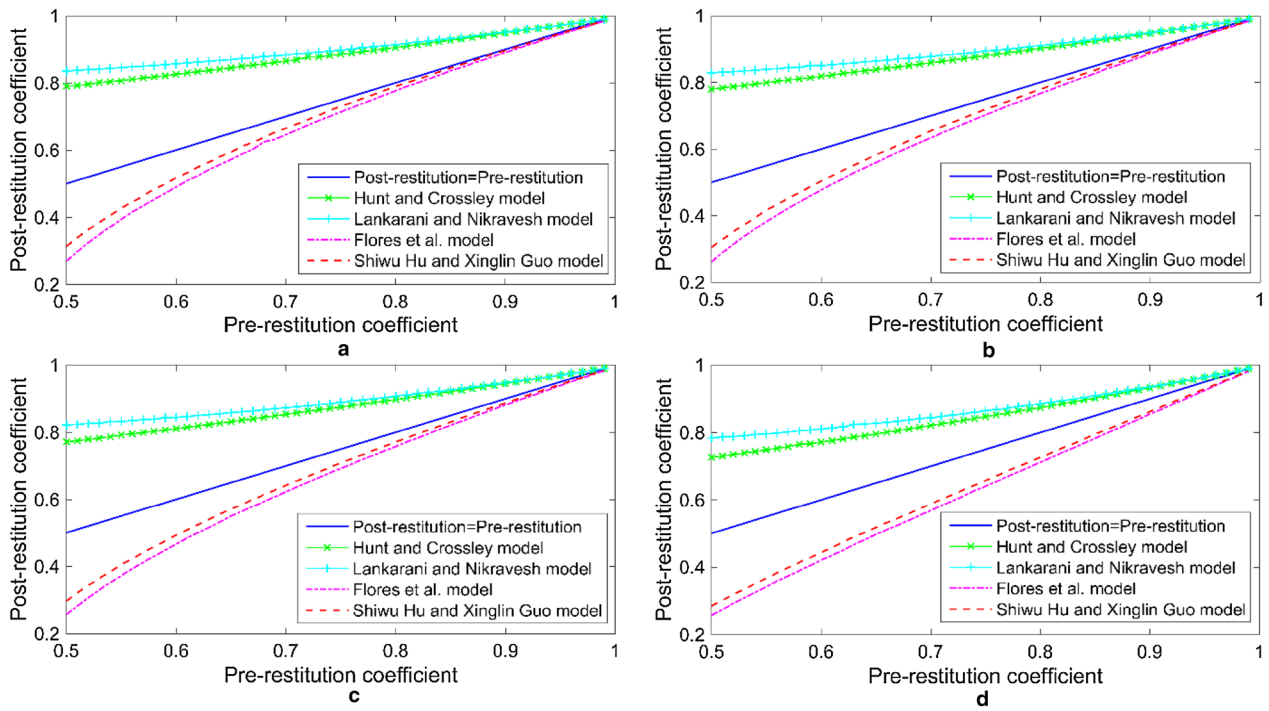

Figure 3 Relation between the post- and pre-restitution coefficients: **a** $\xi_c = -0.022$; **b** $\xi_c = 0.521$; **c** $\xi_c = 0.723$; **d** $\xi_c = 0.941$

the impact damping model needs to be reconsidered for the contact-impact event affected by supporting forces. Since the separation velocity right after contact-impact event cannot be predicted due to the variable end state, the impact damping factor is hard to be modeled, hence Newton method is employed to calculate this factor which obeys the straight line law shown in Figure 3.

For the impact damping factor, a function defined over the real numbers μ can be given in the following form according to Eq. (19) and Eq. (30):

$$f(\mu) = \frac{\int_0^{\delta_m} \left(k_m\delta + \mu\delta\dot{\delta}\right)\mathrm{d}\delta - \left(\int_0^{\delta_m} \mu\delta\dot{\delta}\mathrm{d}\delta + \int_{\delta_m}^{\delta_o} \mu\delta\dot{\delta}\mathrm{d}\delta\right)}{\int_0^{\delta_m} \left(k_m\delta + \mu\delta\dot{\delta}\right)\mathrm{d}\delta} - \varepsilon^2$$
$$= \frac{W_c - \Delta E}{W_c} - \varepsilon^2, \tag{31}$$

where δ_o denotes the deformation at the end of collision. When $f(\mu)$ is equal to zero, the root of this function is the value of μ. Then, the function's derivative is deduced as

$$f'(\mu) = \frac{W_c\left[\int_0^{\delta_m} \delta\dot{\delta}\mathrm{d}\delta - \left(\int_0^{\delta_m} \delta\dot{\delta}\mathrm{d}\delta + \int_{\delta_m}^{\delta_o} \delta\dot{\delta}\mathrm{d}\delta\right)\right] - (W_c - \Delta E)\int_0^{\delta_m} \delta\dot{\delta}\mathrm{d}\delta}{W_c^2}$$
$$= \frac{W_c[S_c - (S_c + S_r)] - (W_c - \Delta E)S_c}{W_c^2} = \frac{\Delta E S_c - W_c(S_c + S_r)}{W_c^2}. \tag{32}$$

With the aid of Eqs. (31) and (32), a better approximation is given by

$$\mu_1 = \mu_0 - \frac{f(\mu_0)}{f'(\mu_0)} = \mu_0 - \frac{\left(1-\varepsilon^2\right)W_{c0}^2 - \Delta E_0 W_{c0}}{\Delta E_0 S_{c0} - W_{c0}(S_{c0} + S_{r0})}, \tag{33}$$

where μ_0 denotes the initial impact damping factor, which is calculated by Shiwu Hu and Xinglin Guo model shown in Table 1. Therefore, the process for the impact damping factor is repeated as

$$\mu_{n+1} = \mu_n - \frac{\left(1-\varepsilon^2\right)W_{cn}^2 - \Delta E_n W_{cn}}{\Delta E_n S_{cn} - W_{cn}(S_{cn} + S_{rn})}, \tag{34}$$

until $|\varepsilon_{post} - \varepsilon_{pre}| \le 0.005\varepsilon_{pre}$ where ε_{post} and ε_{pre} denote the post and pre-restitution coefficient respectively. Consequently, the impact damping model considering supporting forces is

$$D = \mu_{n+1}\delta. \tag{35}$$

Table 1 Impact damping factor models

Model	Factor μ	Model	Factor μ
Hunt and Crossley	$\frac{3(1-\varepsilon)}{2}\frac{k_m}{\delta^{(-)}}$	Flores et al.	$\frac{8(1-\varepsilon)}{5\varepsilon}\frac{k_m}{\delta^{(-)}}$
Lankarani and Nikravesh	$\frac{3(1-\varepsilon^2)}{4}\frac{k_m}{\delta^{(-)}}$	Shiwu Hu and Xinglin Guo	$\frac{3(1-\varepsilon)}{2\varepsilon}\frac{k_m}{\delta^{(-)}}$

4 Application

A start-up and braking process of a helical gear system is taken as an example to illustrate the application of the improved gear contact force model, and then the influence of supporting forces on gear dynamics is also analyzed.

4.1 Model and Computation

A scale model of the high-speed gear train of a type wind turbine gearbox is built in the coordinate system *oxyz*, as shown in Figure 4(a) where the action plane of gear pair is in the *oyz* plane, and the parameters of the model are shown in Table 2. The model consists of driving element, driving gear, driven gear, load element and two driving shafts, wherein, the driving gear is a left spiral helical gear. Due to the less effect of the axial force F_z on the rotation of gear pair, the movement around x-axis is ignored, and the displacements of the y-axis, z-axis and around z-axis direction need to be considered for the two gears. Meanwhile, only around z-axis is considered for the driving and load elements. Thus, the model is an 8-degree freedom transmission system and its displacement vector can be expressed as $\boldsymbol{X}=[\theta_l, y_p, z_p, \theta_p, y_g, z_g, \theta_g, \theta_o]^{\mathrm{T}}$, and then the dynamic equations are given by

$$\ddot{\boldsymbol{X}} = -\boldsymbol{M}^{-1}\boldsymbol{C}\dot{\boldsymbol{X}} - \boldsymbol{M}^{-1}\boldsymbol{K}\boldsymbol{X} + \boldsymbol{M}^{-1}\boldsymbol{P}, \tag{36}$$

with

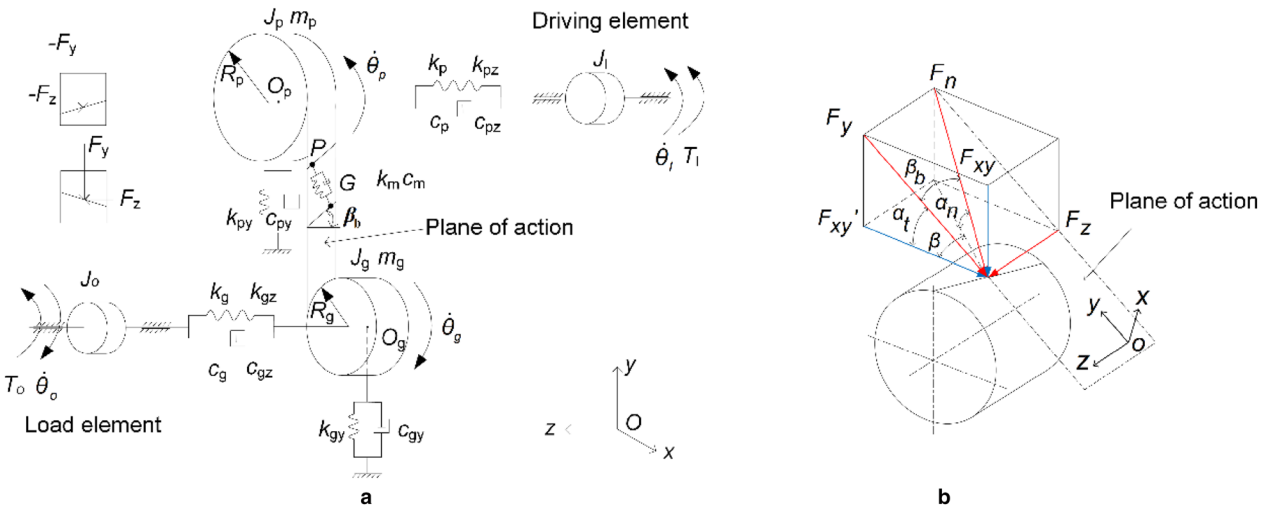

Figure 4 Gear transmission system: **a** dynamic model; **b** action of contact force

Table 2 Properties considered for the transmission system

Property	Value	Property	Value
Teeth number	$z_p=110, z_g=30$	Support damping (N·s/m)	$c_{py}=c_{pz}=6770$
Base radius (m)	$R_p=0.186, R_g=0.051$		$c_{gy}=c_{gz}=5078$
Mass (kg)	$m_p=68, m_g=8.4$	Rotary inertia (N·m·s^2)	$J_p=0.8, J_g=0.007$
Base helix angle (°)	$\beta_b=13.6$		$J_l=0.8323, J_O=1.827$
Backlash (m)	$2b=0.4\times10^{-3}$	Tooth profile error amplitude (m)	$e_a=4\times10^{-6}$
Support stiffness (N/m)	$k_{py}=k_{pz}=3.6\times10^8$,	Tooth profile error wave number	$\upsilon=1$
	$k_{gy}=k_{gz}=2.7\times10^8$	Initial phase (rad)	0
Torsion stiffness (N·m)	$k_p=7.59\times10^5, k_g=6.94\times10^5$	Material coefficient (s/m)	$a=0.3$
Damping coefficient	$\zeta_m=0.05, \zeta_p=\zeta_g=0.02$		

$$\boldsymbol{M}^{-1} = \begin{pmatrix} J_I & 0 & 0 & 0 & 0 & 0 & 0 & 0 \\ 0 & m_p & 0 & 0 & 0 & 0 & 0 & 0 \\ 0 & 0 & m_p & 0 & 0 & 0 & 0 & 0 \\ 0 & 0 & 0 & J_p & 0 & 0 & 0 & 0 \\ 0 & 0 & 0 & 0 & m_g & 0 & 0 & 0 \\ 0 & 0 & 0 & 0 & 0 & m_g & 0 & 0 \\ 0 & 0 & 0 & 0 & 0 & 0 & J_g & 0 \\ 0 & 0 & 0 & 0 & 0 & 0 & 0 & J_o \end{pmatrix},$$

$$\boldsymbol{C} = \begin{pmatrix} c_p & 0 & 0 & -c_p & 0 & 0 & 0 & 0 \\ 0 & c_{py} & 0 & 0 & 0 & 0 & 0 & 0 \\ 0 & 0 & c_{pz} & 0 & 0 & 0 & 0 & 0 \\ -c_p & 0 & 0 & c_p & 0 & 0 & 0 & 0 \\ 0 & 0 & 0 & 0 & c_{gy} & 0 & 0 & 0 \\ 0 & 0 & 0 & 0 & 0 & c_{gz} & 0 & 0 \\ 0 & 0 & 0 & 0 & 0 & 0 & c_g & -c_g \\ 0 & 0 & 0 & 0 & 0 & 0 & -c_g & c_g \end{pmatrix},$$

$$\boldsymbol{K} = \begin{pmatrix} k_p & 0 & 0 & -k_p & 0 & 0 & 0 & 0 \\ 0 & k_{py} & 0 & 0 & 0 & 0 & 0 & 0 \\ 0 & 0 & k_{pz} & 0 & 0 & 0 & 0 & 0 \\ -k_p & 0 & 0 & k_p & 0 & 0 & 0 & 0 \\ 0 & 0 & 0 & 0 & k_{gy} & 0 & 0 & 0 \\ 0 & 0 & 0 & 0 & 0 & k_{gz} & 0 & 0 \\ 0 & 0 & 0 & 0 & 0 & 0 & k_g & -k_g \\ 0 & 0 & 0 & 0 & 0 & 0 & -k_g & k_g \end{pmatrix},$$

$$\boldsymbol{P} = \begin{pmatrix} T_I \\ -F_y \\ -F_z \\ -F_y R_p \\ F_y \\ F_z \\ -F_y R_g \\ T_o \end{pmatrix} = \begin{pmatrix} T_I \\ -F_n \cos\beta_b \\ -F_n \sin\beta_b \\ -F_n R_p \cos\beta_b \\ F_n \cos\beta_b \\ F_n \sin\beta_b \\ -F_n R_g \cos\beta_b \\ T_o \end{pmatrix},$$

where $\ddot{\boldsymbol{X}}$, $\dot{\boldsymbol{X}}$ and $\boldsymbol{X}$ are the acceleration, velocity and displacement vectors, respectively, $\boldsymbol{M}^{-1}$, $\boldsymbol{C}$, $\boldsymbol{K}$, and $\boldsymbol{P}$ denote the mass inverse matrix, the damping matrix, the stiffness matrix, and the force vector. F_y and F_z are the components of F_n on y-axis and z-axis, as shown in Figure 4(b). β, β_b, α_n, and α_t denote the helix angle, the base helix angle, the normal pressure angle, and transverse pressure angle, respectively. The parameter F_n indicates the normal contact force on the pitch circle, and it is calculated by Eq. (1) in which the meshing stiffness shown in Figure 5 is obtained by the approach presented in Section 2 based on Table 2, the deformation and the deformation velocity are given respectively by

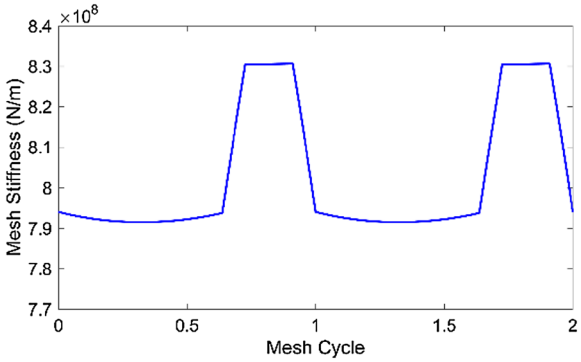

Figure 5 Meshing stiffness

$$\delta = \frac{\bar{y}_p - \bar{y}_g}{\cos\beta_b} - e, \tag{37}$$

$$\dot{\delta} = \frac{\dot{\bar{y}}_p - \dot{\bar{y}}_g}{\cos\beta_b} - \dot{e}, \tag{38}$$

with

$$\bar{y}_p = y_p + z_p \cot\beta_b + \theta_p R_p, \tag{39}$$

$$\bar{y}_g = y_g + z_g \cot\beta_b - \theta_g R_g, \tag{40}$$

where $\bar{y}_p$ and $\bar{y}_g$ denote the displacements of points P and G in the y-axis, respectively, and the negative symbol in the expression of $\bar{y}_g$ indicates the opposite rotation direction of driven gear to driving gear. Assuming the static transmission error is caused by the driven gear, the static transmission error e and its rate $\dot{e}$ are expressed as

$$e = e_a \sin\left(\theta_g \upsilon z_2 + q\right), \tag{41}$$

$$\dot{e} = e_a \upsilon z_2 \frac{\dot{\theta}_g}{2\pi} \cos\left(\theta_g \upsilon z_2 + q\right), \tag{42}$$

in which e_a denotes the fluctuation amplitude, υ represents the error rate wave number of single tooth, z_2 and q illustrate the tooth number of driven gear and the initial phase, respectively. For the restitution coefficient Eq. (43) represented in Ref. [18] is also adopted in this study

$$\varepsilon = 1 - \alpha \dot{\delta}^{(-)}, \tag{43}$$

in which α is the coefficient of material.

The four order Runge–Kutta method is applied to solve Eq. (36), and the numerical computation process is proposed, as shown in Figure 6 where F_n, c_m, and μ_{n+1} are computed by Eqs. (1), (17), and (34), respectively. According to the operation conditions of the wind turbine gearbox, the input and output torque of the transmission

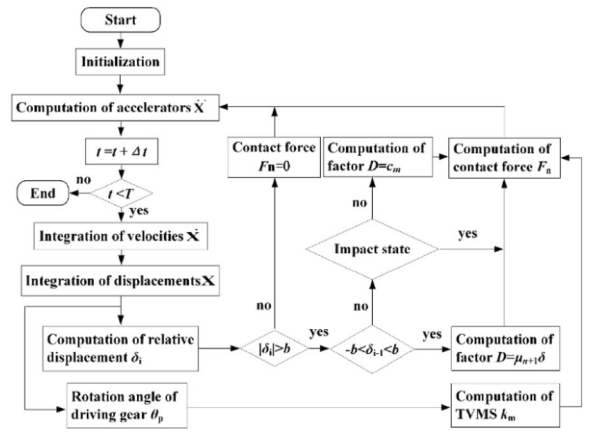

Figure 6 Numerical computation process

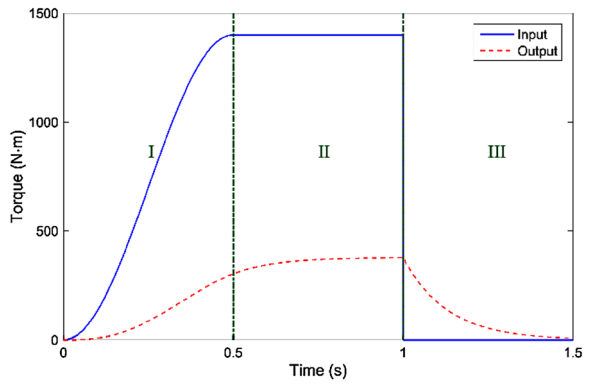

Figure 7 Input and output torques

system shown in Figure 7 are set, and then the simulation is carried out for the dynamic response analysis of the gear system.

4.2 Development of Gear Pair State

In the process of gear transmission, the gear pair is not always in normal meshing state due to the influence of backlash and external loads, and sometimes its behavior reflects strong non-linear dynamic characteristics [31, 32]. Under the working condition shown in Figure 7, the gear pair undergoes a development process from abnormal meshing state to smooth meshing state, and then from smooth meshing state to abnormal meshing state until to stop, as shown in Figure 8(a). The curve is the ratio between δ obtained by Eq. (36) and 0.5 times backlash b, that is δ/b. According to the judgement of gear pair state, the gear pair is in contact state when the ratio is greater than 1 or less than -1, and the deformation is $|\delta|-b$; The gear pair is in contact loss state when the ratio is greater than -1 and less than 1; At the moment of the absolute value of the ratio passes through 1 and greater than 1, the contact-impact event takes place; Then the gear pair enters contact loss state again or normal meshing state at the end of contact-impact event. Overall, in the start-up stage, there are several continuous contact-impact phenomena, and then followed by a stable normal meshing state. During the brake stage, the gear pair collides repeatedly between front tooth surface and back tooth surface, and it also exhibits vibration attenuation phenomenon.

For the phenomena of contact-impact event, the more details are shown in Figure 8(b) where the symbols "o"

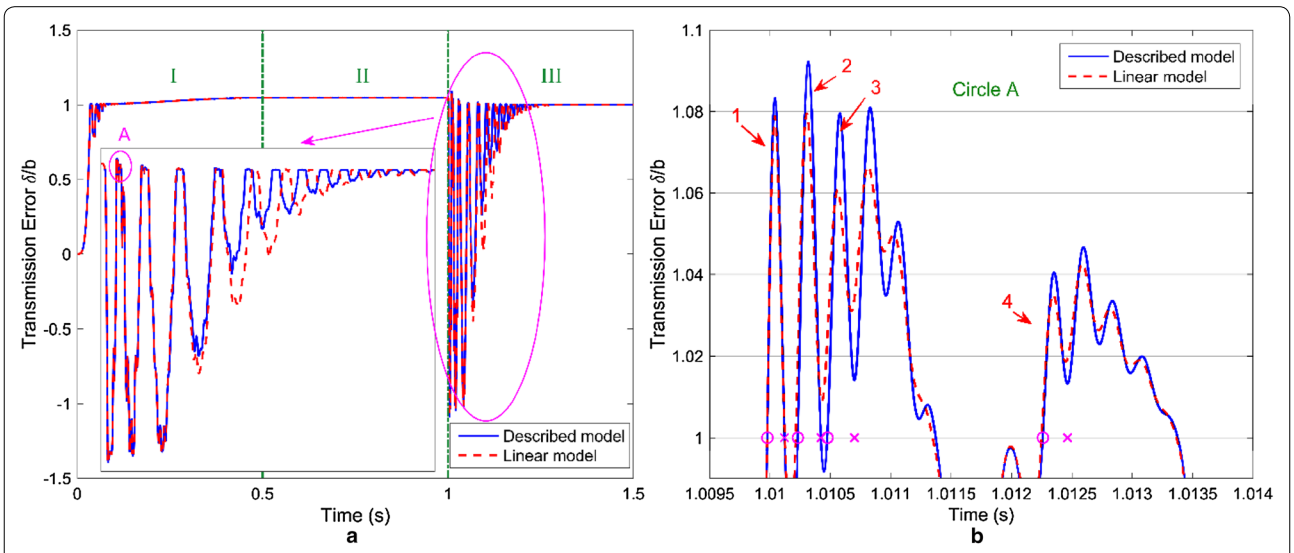

Figure 8 Transmission error ratio δ/b

and "×" denote the start mark and the end mark of contact-impact event, respectively. This figure shows the gear pair undergoes a repeated contact-impact process before a normal meshing state.

4.3 Influence of Supporting Forces on Dynamic Response

It can also be drawn from Figure 8(a) that the difference between solid line and dotted line which are obtained by the described model and the linear spring damping model, respectively, increases firstly and then decrease. Figure 8(b), which is the ratio curve of the circle A, shows the detailed difference between these two models. It is apparent that the solid line shows four collisions, whereas the dotted line exhibits three. In fact, this different response which has been represented in Ref. [18] is caused by the accumulative error in the dissipative energy of each collision between these two force models.

As aforementioned, the energy loss during collision and the impact end state are influenced by the effect factor ξ_c and ξ_r, respectively, thus, these two factor are plotted in Figure 9 for detailed analysis. This figure illustrates that most effect factors ξ_c during each collision are large than 0.3 which means the large effect of supporting force. For instance, the initial relative velocity of the

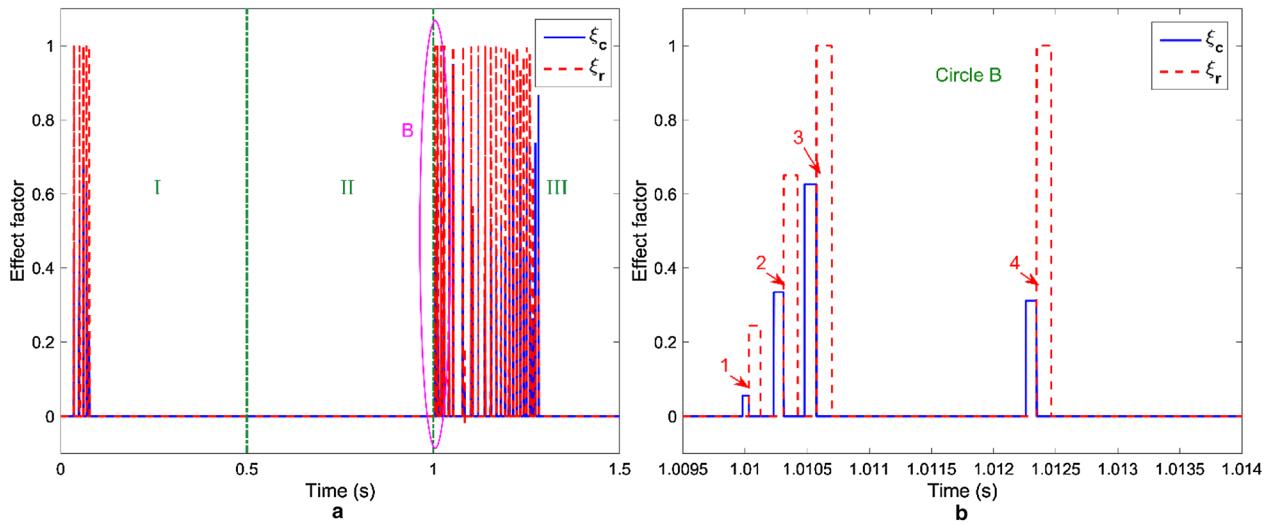

Figure 9 Developments of influence factor

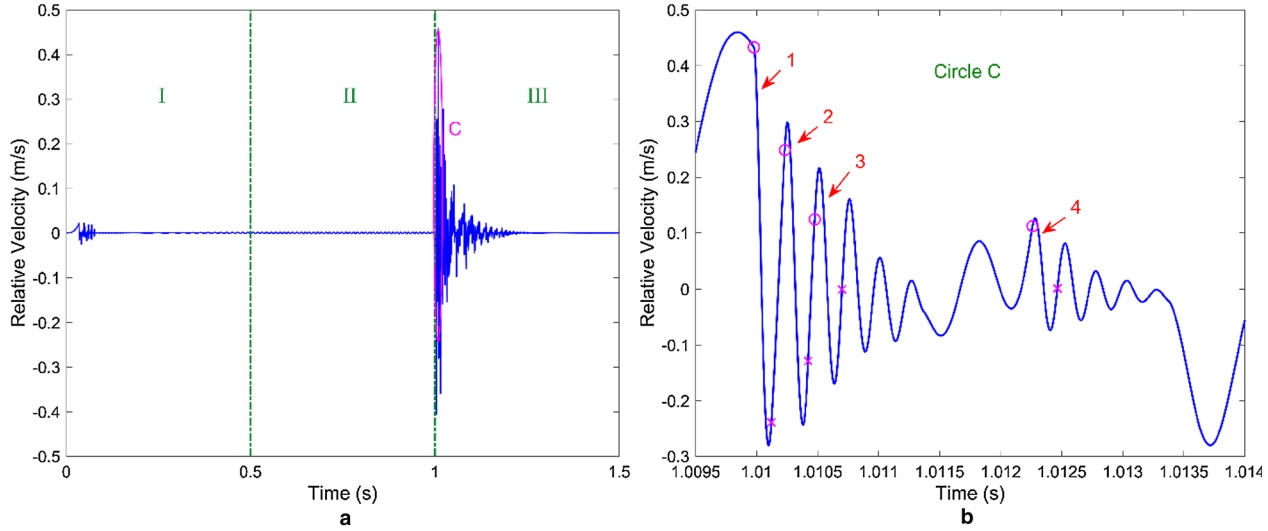

Figure 10 Development of relative velocity

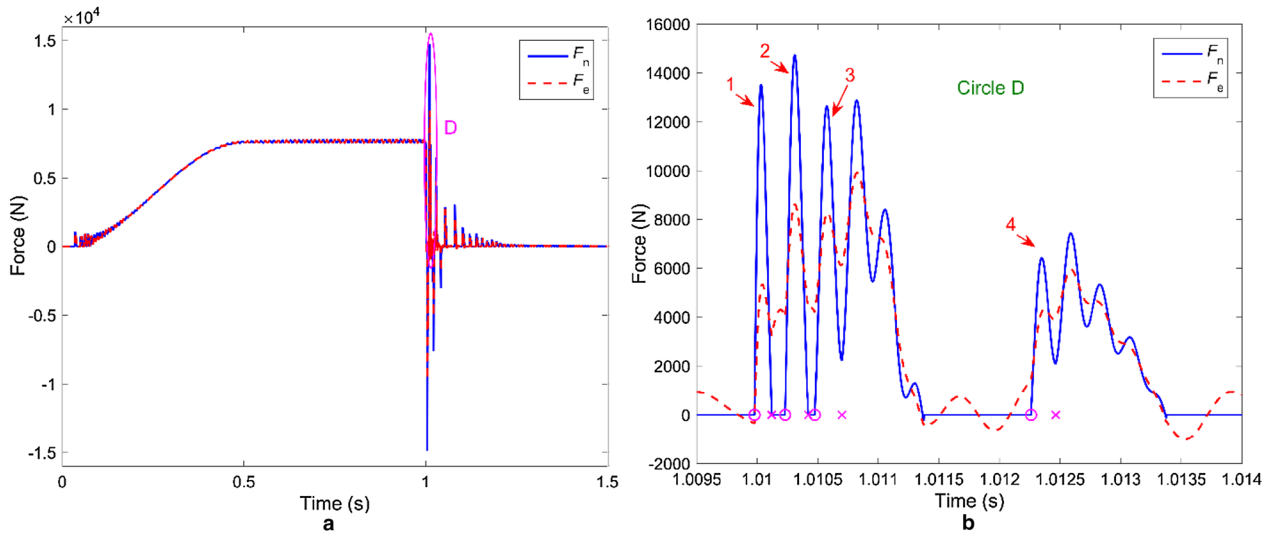

Figure 11 Developments of contact force and equivalent supporting force

first collision is larger than the second collision, as shown in Figure 10(b), however the corresponding maximum contact force is smaller, as shown in Figure 11(b), since the effect factor ξ_c of the second collision is large than 0.3 while the first collision is less than 0.1. According to Eq. (22), this phenomenon can be explained that the maximum elastic strain energy is transferred from the initial relative motion and the work done by supporting forces on deformation. In other words, the maximum contact-impact force is affected by both initial relative velocity and supporting forces, and the large effect factor ξ_c can obviously influence on impact force. For the deformation velocity, this influence is also obvious, such as the second and the third collisions. Figure 9 also shows that the effect factor ξ_r is equal to 1 when gear pair enters normal meshing state from impact state, which can also be concluded by Eq. (26).

In conclusion, the contribution of supporting forces is important to the deformation, deformation velocity, contact force, and dissipative energy of contact-impact event. The contact-impact force model considering the influence of supporting forces is necessary for the simulation of gear transmission system.

5 Conclusions

In this paper, the issue of contact force model considering the normal meshing and contact-impact states was analyzed for helical gear system. As the basic problem, the time-varying meshing stiffness and the meshing damping were discussed for the normal meshing state, and the collision evolution associated with fundamental contact mechanics was also investigated. Furthermore, the influence of supporting forces on collision, including deformation velocity, dissipative energy and impact end state, was analyzed. Especially, a new model of restitution coefficient was deduced for both separation and non-separation states. According to this new model and the Newton method, a hysteresis damping factor was derived for calculating impact damping force. In order to better understand the described method proposed in this paper, a dynamic analysis of a helical gear system was carried out under start-up and braking conditions. In this analysis, the specific application of the described model was represented with the computation process of the helical gear system. The results showed that: (1) the described contact force model is more suitable for dynamics analysis in gear system; (2) the gear pair undergoes a repeated contact-impact process before entering normal meshing state; (3) the contribution of supporting forces is important to impact force, deformation velocity and energy loss during collision when $\xi_c > 0.3$; 4) supporting forces and dissipative energy are the main reasons for gear system to enter a steady contact state from repeated impact state.

Authors' Contributions

DX was in charge of the whole trial; YS wrote the manuscript; YW assisted with simulation and writing manuscript. All authors read and approved the final manuscript.

Authors' Information

Dong Xiang, is currently an associate professor at *Department of Mechanical Engineering, Tsinghua University, Beijing, China.*

Yinhua Shen, is currently a PhD candidate at *Department of Mechanical Engineering, Tsinghua University, China.*

Yaozhong Wei, is currently a master candidate at *Department of Mechanical Engineering, Tsinghua University, China.*

Competing Interests
The authors declare that they no competing interests.

Funding
Supported by National Natural Science Foundation of China (Grant No. 51475263).

Received: 13 January 2019 Accepted: 22 April 2019
Published online: 05 May 2019

References

[1] P Flores, M Machado, M T Silva, et al. On the continuous contact force models for soft materials in multibody dynamics. *Multibody Syst. Dyn.*, 2011, 25(3): 357-375.
[2] M Inalpolat, M Handschuh, A Kahraman. Influence of indexing errors on dynamic response of spur gear pairs. *Mechanical Systems and Signal Processing*, 2015, 60-61: 391-405.
[3] S Zhou, G Song, Z Ren, et al. Nonlinear dynamic analysis of coupled gear-rotor-bearing system with the effect of internal and external excitations. *Chinese Journal of Mechanical Engineering*, 2016, 29(2): 281-292.
[4] A Fernandez-Del-Rincon, A Diez-Ibarbia, S Theodossiades. Gear transmission rattle: Assessment of meshing forces under hydrodynamic lubrication. *Applied Acoustics*, 2017, 144: 85-95.
[5] Y A Khulief, A A Shabana. A continuous force model for the impact analysis of flexible multibody systems. *Mechanism and Machine Theory*, 1987, 22(3): 213-224.
[6] A Kahraman, R Singh. Non-linear dynamics of a spur gear pair. *Journal of Sound and Vibration*, 1990, 142(1): 49-75.
[7] Y Wen, J Yang, S Wang. Random dynamics of a nonlinear spur gear pair in probabilistic domain. *Journal of Sound and Vibration*, 2014, 333(20): 5030-5041.
[8] F H Liu, S Theodossiades, L A Bergman, et al. Analytical characterization of damping in gear teeth dynamics under hydrodynamic conditions. *Mechanism and Machine Theory*, 2015, 94: 141-147.
[9] Z Hu, J Tang, J Zhong, et al. Effects of tooth profile modification on dynamic responses of a high speed gear-rotor-bearing system. *Mechanical Systems and Signal Processing*, 2016, 76-77: 294-318.
[10] J Zhan, M Fard, R Jazar. A CAD-FEM-QSA integration technique for determining the time-varying meshing stiffness of gear pairs. *Measurement*, 2017, 100: 139-149.
[11] X H Liang, Z L Liu, J Pan, et al. Spur gear tooth pitting propagation assessment using model-based analysis. *Chinese Journal of Mechanical Engineering*, 2017, 30(6): 1369-1382.
[12] K H Hunt, F R E Crossley. Coefficient of restitution interpreted as damping in vibroimpact. *Journal of Applied Mechanics*, 1975, 42(2): 440-445.
[13] T W Lee, A C Wang. On the dynamics of intermittent-motion mechanisms. Part 1: Dynamic model and response. *Journal of Mechanisms, Transmissions, and Automation in Design*, 1983, 105(3): 534-540.
[14] H M Lankarani, P E Nikravesh. A contact force model with hysteresis damping for impact analysis of multibody systems. *Journal of Applied Mechanics*, 1990, 112(3): 369-376.
[15] Y Gonthier, J McPhee, C Lange, et al. A regularized contact model with asymmetric damping and dwell-time dependent friction. *Multibody System Dynamics*, 2004, 11(3): 209-233.
[16] S Hu, X Guo. A dissipative contact force model for impact analysis in multibody dynamics. *Multibody System Dynamics*, 2015, 35(2): 131-151.
[17] D Xing, Y H Shen, Y Z Wei, et al. A comparative study of the dissipative contact force models for collision under external spring forces. *Journal of Computational and Nonlinear Dynamics*, 2018, 13(10): 101009.
[18] Y H Shen, D Xing, Y Z Wei, et al. A contact force model considering constant external forces for impact analysis in multibody dynamics. *Multibody System Dynamics*, 2018, 44(4): 397-419.
[19] H Ma, J Zeng, R Feng, et al. Review on dynamics of cracked gear systems. *Engineering Failure Analysis*, 2015, 55: 224-245.
[20] F L Litvin, A Fuentes, I Gonzalez-Perez, et al. Modified involute helical gears: computerized design, simulation of meshing and stress analysis. *Computer Methods in Applied Mechanics and Engineering*, 2003, 192(33-34): 3619-3655.
[21] D C H Yang, J Y Lin. Hertzian damping, tooth friction and bending elasticity in gear impact dynamics. *Journal of Mechanisms, Transmissions, and Automation in Design*, 1987, 109(2): 189-196.
[22] Q Wang, Y Zhang. A model for analyzing stiffness and stress in a helical gear pair with tooth profile errors. *Journal of Vibration and Control*, 2017, 23(2): 272-289.
[23] Q Wang, B Zhao, Y Fu, et al. An improved time-varying meshing stiffness model for helical gear pairs considering axial mesh force component. *Mechanical Systems and Signal Processing*, 2018, 106: 413-429.
[24] H Ma, R Song, X Pang, et al. Time-varying meshing stiffness calculation of cracked spur gears. *Engineering Failure Analysis*, 2014, 44: 179-194.
[25] P Sainsot, P Velex, O Duverger. Contribution of gear body to tooth deflections-a new bidimensional analytical formula. *Journal of Mechanical Design*, 2004, 126(4): 748-752.
[26] N Yousfi, B Zghal, A Akrout, et al. Damping models identification of a spur gear pair. *Mechanism and Machine Theory*, 2018, 122: 371-388.
[27] R Kasuba, J W Evans. An Extended model for determining dynamic loads in spur gearing. *Journal of Mechanical Design*, 1981, 103: 398-409.
[28] S Chen, J Tang, L Wu. Dynamics analysis of a crowned gear transmission system with impact damping: Based on experimental transmission error. *Mechanism & Machine Theory*, 2014, 74: 354-369.
[29] J Alves, N Peixinho, M T Da Silva, et al. A comparative study of the viscoelastic constitutive models for frictionless contact interfaces in solids. *Mechanism & Machine Theory*, 2015, 85: 172-188.
[30] W J Stronge. Rigid body collisions with friction. *Proceedings of the Royal Society of London, Series A: Mathematical and Physical Sciences*, 1990, 431(1881): 169-181.
[31] R G Parker, X Wu. Vibration modes of planetary gears with unequally spaced planets and an elastic ring gear. *Journal of Sound and Vibration*, 2010, 329: 2265-2275.
[32] P M T Marquesa, R C Martinsa, J H O Seabrab. Gear dynamics and power loss. *Tribology International*, 2016, 97: 400-411.